



Parametric Analysis of Borehole Breakout and Spalling Phenomena: An Experimental Investigation

Zizhuo Xiang¹ · Joung Oh¹ · Guangyao Si¹ · Ismet Canbulat¹

Received: 31 January 2024 / Accepted: 22 April 2024
© The Author(s) 2024

Abstract

This study investigated borehole breakout and spalling phenomena through true-triaxial experiments conducted on cubic Gosford sandstone and yellow mudstone specimens. The experiments were carried out based on the custom-developed borehole breakout testing system, which could enable the pre-stressed (PS) tests (applying stresses onto intact specimens and then drilling). In comparison to the pre-drilled (PD) tests (applying stresses onto specimens with pre-drilled boreholes), the PS tests consistently resulted in wider and deeper breakouts under the same far-field stresses in both rock types, which are attributed to the impacts of excavation-unloading and removal of rock debris. The results from 36 PS tests indicated that the breakout and spalling extent are affected by all three principal stresses, and the impact of each stress was also quantitatively assessed and compared. Moreover, analysis of experimental data from this study and the literature revealed that a unique correlation between breakout angle and normalised breakout depth could not be obtained, suggesting deriving two principal stress components from two breakout geometries should be viable. Furthermore, empirical correlations based on the maximum tangential stress (σ_{max}) and out-of-plane stress were developed to characterise the breakout geometries, which outperformed those previous relations based solely on σ_{max} across all datasets. This suggests that while the breakout and spalling phenomena are primarily controlled by σ_{max} , a more accurate representation of failure extent can be achieved by considering the out-of-plane stress.

Highlights

- Borehole breakout experiments were conducted on sandstone and mudstone through a custom-designed true-triaxial testing system.
- The impacts of testing methodologies and the magnitude of each principal stress on breakout geometries were analysed in both rock types.
- The correlation between breakout angle and normalised breakout depth was investigated based on six pre-stressed datasets.
- Empirical equations based on the maximum tangential stress and out-of-plane stress were developed to characterise the breakout geometries.

Keywords Borehole breakout · Spalling · True-triaxial experiment · Drilling under loading · Intermediate principal stress

1 Introduction

Breakout and spalling are localised failures occurring in the vicinity of underground openings as a result of drilling and excavation under high far-field stress conditions. Figure 1 illustrates a schematic diagram of the typical borehole breakout around vertical boreholes. The failures manifest as V-shaped zones along the minimum horizontal stress direction, which can be characterised by two geometrical parameters, breakout angle (θ_b) and normalised breakout depth

✉ Joung Oh
joung.oh@unsw.edu.au

¹ School of Minerals and Energy Resources Engineering,
University of New South Wales, Sydney, NSW 2052,
Australia

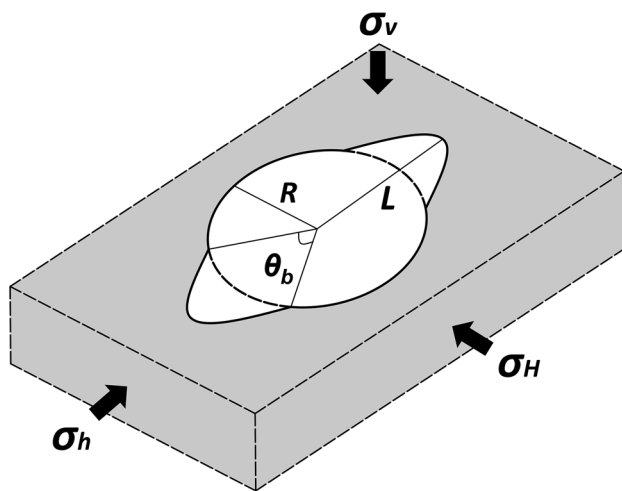


Fig. 1 A schematic diagram of borehole breakout. (σ_H : maximum horizontal stress, σ_h : minimum horizontal stress, σ_v : vertical stress, θ_b : breakout angle, L : breakout depth, R : borehole radius)

(L/R). The phenomenon was first observed by Cox (1972) through a borehole dipmeter as elongations on both sides of the borehole. As the excavation continues to proceed toward greater depths, breakout and spalling phenomena have been widely observed in openings of various sizes across civil, petroleum and mining operations (Zoback et al. 1985; Emmermann and Lauterjung 1997; Martin 1997; Hoek and Martin 2014; Feng et al. 2018).

Extensive studies have been carried out aiming to understand the breakout and spalling mechanisms, among which, in-situ tests can provide the most realistic representation of failure formation. The Mine—by experiment in Canada thoroughly described the progressive failure formation and investigated the impact of stress path on the rock strength (Martin 1997; Martin et al. 1997; Read 2004). Subsequently, the Äspö pillar stability test was conducted to further investigate the impact of excavation—and thermal-induced stresses on the spalling behaviour to quantify the rock spalling strength (Andersson et al. 2009; Andersson and Martin 2009). Based on in-situ observations, an empirical correlation was proposed to estimate the spalling depth for tunnel stability analysis and excavation support design based on the ratio of maximum stress on the tunnel wall and rock strength (Martin et al. 1999, 2001; Martin and Christiansson 2009). Given the difficulties of in-situ testing, laboratory experiments have also been conducted on cubic samples under polyaxial loading conditions primarily using two testing methodologies: the pre-drilled (PD) method (drilling prior to loading) (Lee and Haimson 1993; Cheon et al. 2011; Hu et al. 2019; Ling et al. 2023) and pre-stressed (PS) method (loading prior to drilling) (Haimson 2007; Si et al. 2022;

Xiang et al. 2023d). Although the former allows more comprehensive monitoring of the breakout formation process, Xiang et al. (2023d) demonstrated that the latter would yield greater θ_b and L/R due to excavation unloading and removal of rock debris by drilling fluid/vibration. Nevertheless, additional experimental investigations are required to further verify the differences between the two methods. Moreover, while the influences of all three principal stresses on the peak rock strength have been well documented (Mogi 1967; Colmenares and Zoback 2002; You 2009), research on borehole breakout is still primarily focused on the in-plane stresses (mostly σ_H). The impact of the out-of-plane stress (i.e., σ_v in Fig. 1) is yet to be fully explored and integrated into practice.

Borehole breakout and spalling phenomena have been proven to contain critical geotechnical information related to far-field stresses. Breakout has been widely employed as an indicator for stress orientation since it would align with the σ_h direction in the absence of geological structures (Gough and Bell 1981; Barton et al. 1988; Zoback et al. 2003; Stephansson and Zang 2012). Furthermore, given the stress dependence on rock failure dimensions, attempts have been carried out to constrain and inverse in-situ stresses based on breakout geometries (Zoback et al. 2003; Song and Chang 2018; Lin et al. 2020; Han and van der Baan 2024). However, based on experimental and numerical investigations, some researchers suggested that there could be a unique correlation between the two breakout geometries (Haimson et al. 1991; Haimson and Lee 2004; Sahara et al. 2017). Consequently, under this hypothesis, only one in-plane stress component could be estimated from borehole breakout geometries. Nonetheless, these analyses were primarily based on limited data from single rock types. To comprehensively explore the correlation between θ_b and L/R , further investigation using data from different stress conditions and rock types is required.

In this study, true-triaxial borehole breakout experiments were carried out on two rock types, sandstone and mudstone. The differences in the failure dimensions between the two testing methodologies, PD and PS, were quantified and analysed. The impact of each principal stress on the breakout geometries was systematically assessed through seven sets of PS experiments. Based on the experimental results and data collected from past studies, the correlation between θ_b and L/R across different datasets was assessed, and empirical correlations between the breakout geometries and far-field stresses were proposed by considering all principal stresses. The results of this study are expected to provide new insights into the formation mechanism and stress dependency of borehole breakout and spalling.

2 Methodology

2.1 Rock Specimens

Two types of rocks were utilised for the borehole breakout experiments: Gosford sandstone (GSS) from Sydney Basin (Fig. 2a) and yellow mudstone (YMS) from Victoria (Fig. 2b), Australia. The rock mechanical properties were tested and summarised in Table 1, following the ISRM suggested methods (Bieniawski and Hawkes 1978; Bieniawski and Bernede 1979; Franklin 1979). Cubic specimens with a side dimension of 120 mm were prepared for true-triaxial testing. The sample surface was ground to yield flat and mutually perpendicular surfaces. The rock specimens could be considered isotropic and free of notable bedding characteristics based on visual observations and mechanical tests.

2.2 Experimental Setup and Procedure

The experiments were carried out at the University of New South Wales, Sydney, by the custom-developed true-triaxial borehole breakout testing system (Fig. 3), consisting of an MTS 815 loading frame, a biaxial compression cell and a servo-controlled drilling assembly. The major principal stress is applied to the sample through the MTS 815 testing frame (up to 1500 kN), and the intermediate and minor principal stresses are loaded by the biaxial compression cell (up to 550 kN). The servo-controlled drilling assembly, which was designed in-house, enables automated drilling with adjustable drilling speed. A diamond core bit with a 22 mm outer diameter was utilised in the drilling process.

Table 1 Mechanical properties of the tested rocks

Rock properties	GSS	YMS
Density (kg/m^3)	2184.9 ± 27.6	2364.8 ± 5
Uniaxial compressive strength (<i>UCS</i>) (MPa)	36.4 ± 2.9	104.1 ± 10.6
Brazilian tensile strength (<i>BTS</i>) (MPa)	2.1 ± 0.6	4.9 ± 0.7
Young's modulus (GPa)	6.9 ± 0.6	13.9 ± 1.4
Poisson's ratio	0.20 ± 0.02	0.24 ± 0.01
Porosity (%)	16.9 ± 0.9	10.9 ± 0.9

Both PD and PS methodologies were adopted in the experiments. In the PD tests, true-triaxial stresses were loaded onto the specimen with a prefabricated borehole (22 mm in diameter), following the common loading paths described in Feng et al. (2019). Once the targeted stresses were installed, the stress condition was kept for an additional 30 min period to allow the formation and stabilisation of the breakout and spalling. A borehole camera was inserted throughout the experiment to record the failure process. On the other hand, in the PS test, true-triaxial stresses were applied to an intact specimen through the same loading procedure as the PD test. Borehole drilling was conducted approximately 10 min after the stress installation and equilibrium, with an advance rate of 0.33 mm/s. During drilling, water was circulated (0.017–0.02 L/s) through the drill bit and borehole to cool down the drill bit and remove rock debris. Upon completion of the drilling, the drill bit was carefully retracted, and the sample was then maintained under the same stress state for an additional 30 min. Note that in all experiments, the drilling direction was assumed

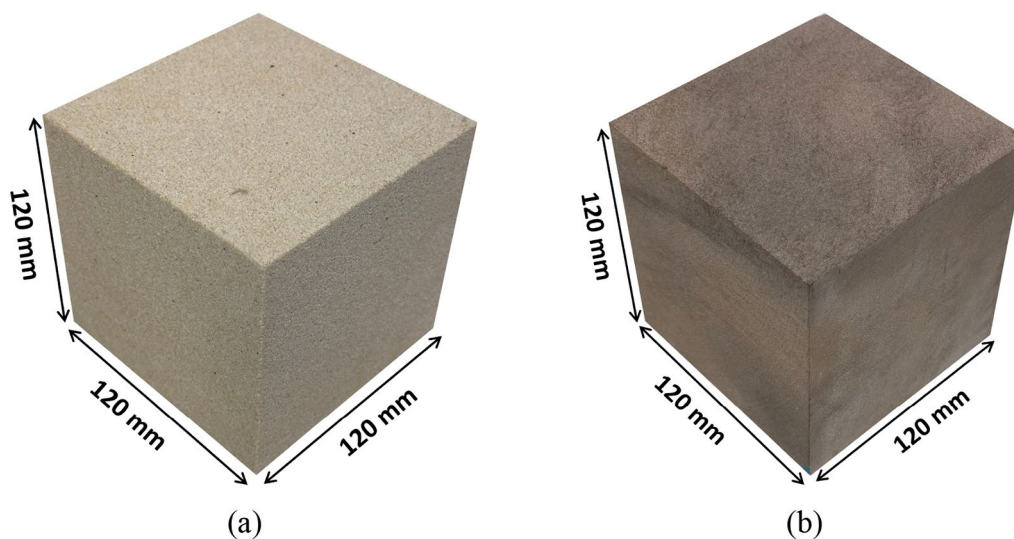


Fig. 2 Rock specimens for the borehole breakout experiments: **a** GSS and **b** YMS

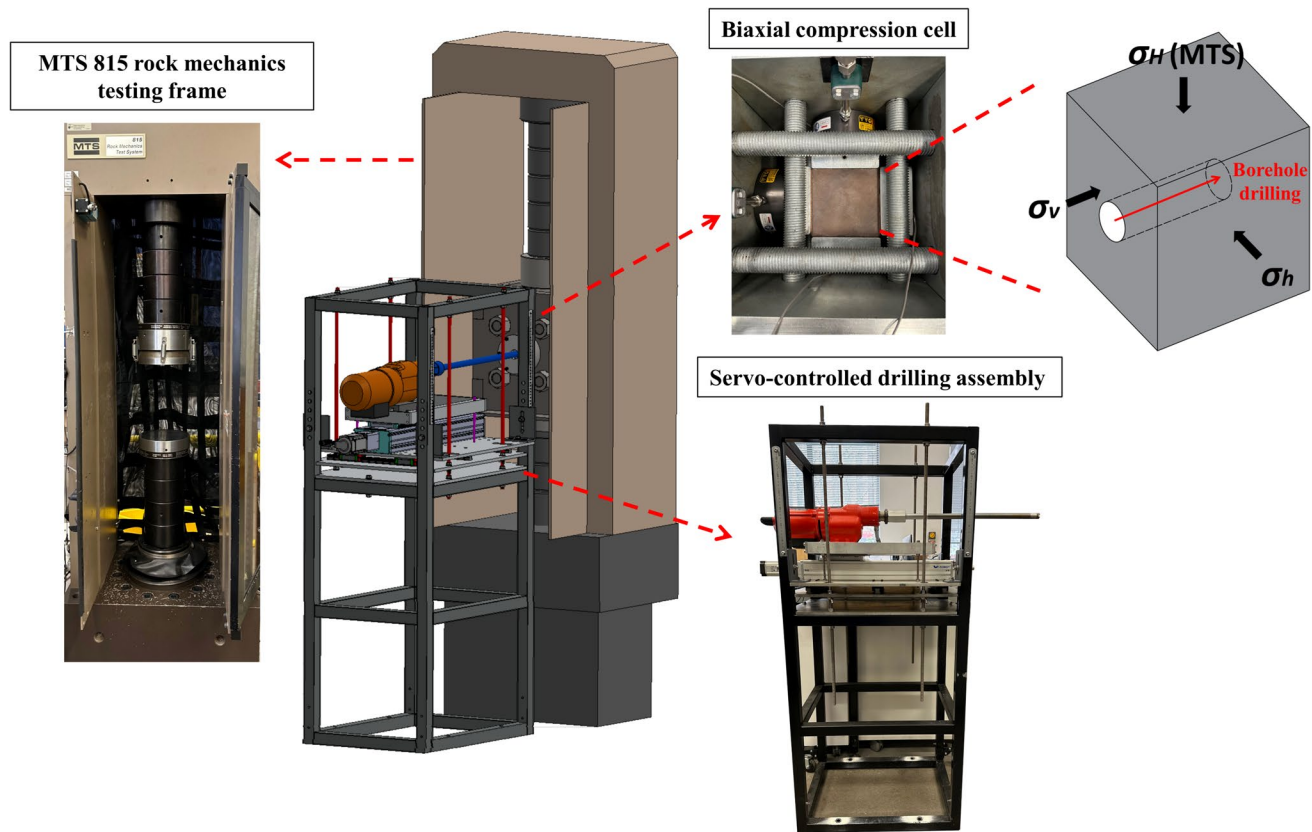


Fig. 3 Experimental setup for true-triaxial borehole breakout tests

to be aligned with the σ_v direction (Fig. 3), mimicking the breakout formation in vertical boreholes.

After completing the experiment, the sample was removed from the testing system. For the breakout geometries extraction, the sample was carefully cut along the σ_H direction and subsequently taken for 3D scanning (Fig. 4) using the Shining 3D EinScan Pro 2X scanner to obtain the breakout profiles (accuracy up to 0.04 mm). The final breakout geometries were determined by averaging the values from both sides of the borehole.

3 Experimental Results and Analysis

3.1 Comparison of PD and PS Experiments

Determining the appropriate experimental method (PD or PS) is crucial for investigating borehole breakout and spalling phenomena. The disparities between the PD and PS experiments on GSS have been systematically discussed in Xiang (2023d). This section extends the analysis to include six additional experiments (three PD and three PS) performed on YMS, and the differences between the two testing methods on the two rock types are analysed.

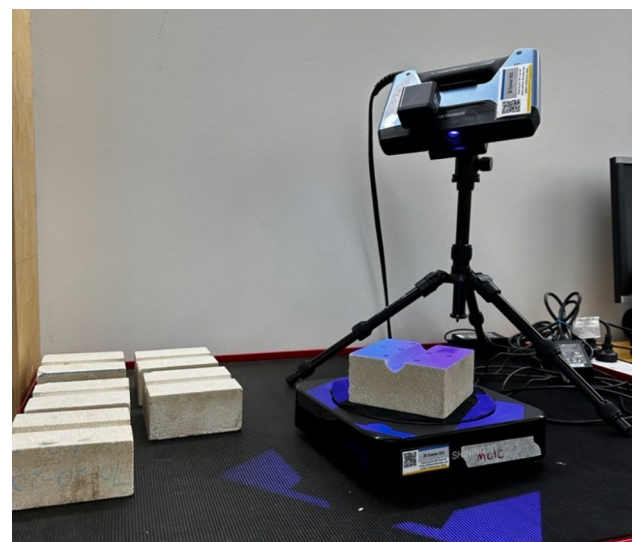


Fig. 4 3D scanning of the tested specimens

The borehole recordings for GSS ($\sigma_H = 70$ MPa, $\sigma_h = 25$ MPa, $\sigma_v = 20$ MPa) and YMS ($\sigma_H = 90$ MPa, $\sigma_h = 15$ MPa, $\sigma_v = 10$ MPa) from PD tests are depicted in Fig. 5. Note that the different stress conditions applied to

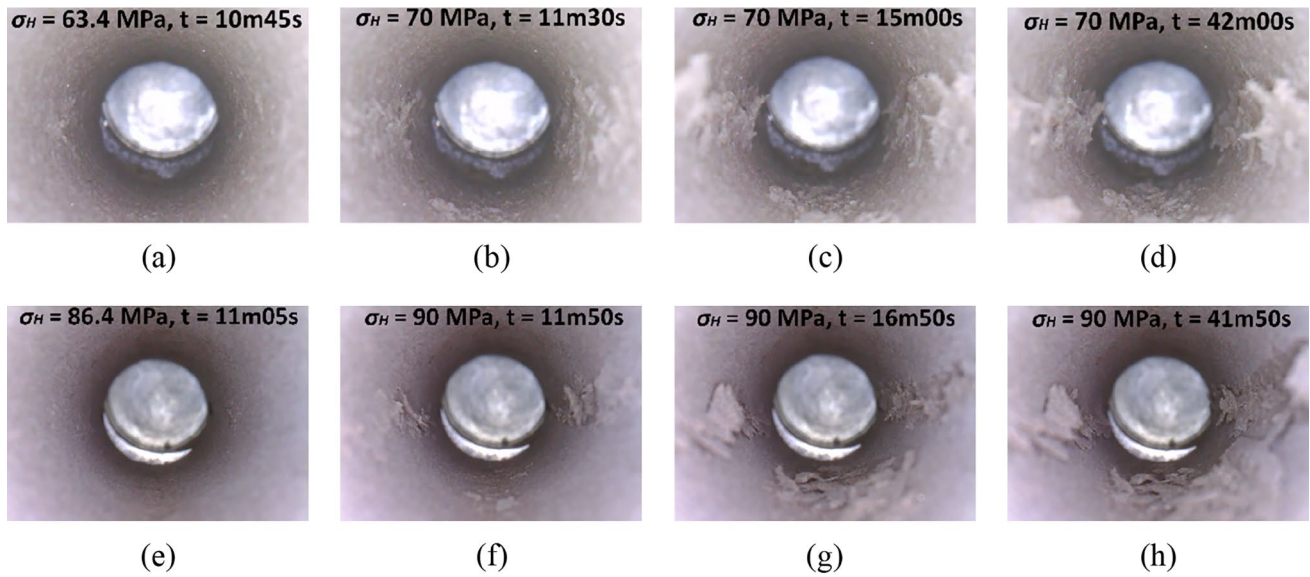


Fig. 5 Breakout evolution process of PD experiments in **a–d** GSS ($\sigma_h = 25$ MPa, $\sigma_v = 20$ MPa) and **e–h** YMS ($\sigma_h = 15$ MPa, $\sigma_v = 10$ MPa)

GSS and YMS are attributed to their different mechanical properties. More specifically, YMS specimens have significantly higher strength compared to GSS, which would require greater differential stresses to induce breakout. Overall, the borehole failure in GSS predominantly occurred in the forms of buckling deformation and grain ejection associated with a small number of rock slabs peeling off from the failure zones. On the other hand, the breakout formation process in YMS differed slightly. The failure initiated at around $\sigma_H = 75$ MPa, with slight bulging observed on the right borehole wall. Damage occurred on the left sidewall when σ_H reached 78 MPa, and rock grains began to be ejected from the failure area as the stress continued to increase. At $\sigma_H = 86.4$ MPa, rock slabs started to form and subsequently ejected and detached from the sidewalls. The intensity of the breakout development

continuously grew until 4–5 min after σ_H reached its target value (90 MPa). Afterwards, the rock slabbing and ejection gradually ceased, and the rock fragments slowly peeled off under gravity instead of being ejected in the rest of the experiment. In contrast to the sandstone, side-wall failure in YMS manifested more in the form of slab ejection with a higher ejecting velocity (Fig. 6), resulting in less debris remaining at the breakout locations. Furthermore, spalled rock fragments in YMS were generally larger. Consequently, toward the end of the experiment, a V-shaped failure zone could be observed on the right side of the borehole (Fig. 5h) as opposed to the protruding rock debris observed in GSS (Fig. 5d). Furthermore, the failure surface in YMS appeared smoother than that of GSS, indicating the potential presence of more tensile cracks in YMS breakout.

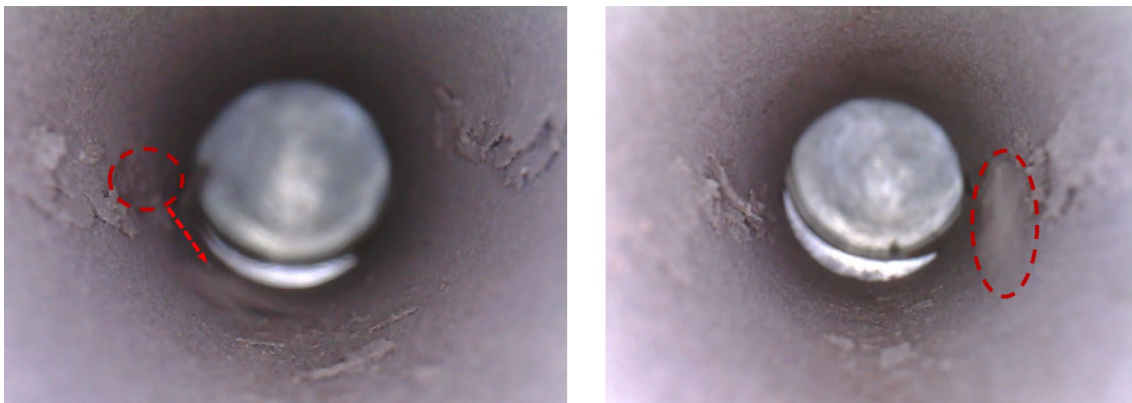


Fig. 6 Rock slab ejection in YMS

The boreholes in the PS tests exhibited notably different breakout patterns compared to those under the PD conditions, despite the same far-field stresses. Examples of the breakout images obtained from both testing methodologies are given in Fig. 7. In the PS experiments, symmetrical V-shaped failure zones can be observed on both sides of the borehole walls, which are considerably wider and deeper in contrast to the PD breakouts. Additionally, no visible rock fragments are observed at the failure area in the PS conditions, which is consistent with the field observations through borehole logs (Borm et al. 1997; Tingay et al. 2008). Furthermore, core discing phenomena are also observed in PS tests under relatively high σ_H (Fig. 8).

Post-experiment, debris at the breakout locations of the PD samples was carefully removed, and the breakout geometries of the PD and PS samples were obtained. As indicated in Fig. 9, both breakout geometries from the PS tests are consistently greater than those of the PD tests, and the

discrepancies are evident in both rock types. The average variations in θ_b for YMS and GSS are similar at approximately 10.2 and 12.5°, respectively. As for L/R , the difference in GSS increases significantly with the magnitudes of σ_H , whereas the values remain relatively constant for YMS at around 0.11.

The discrepancies in the failure extent between the two testing conditions are believed to be attributed to the stress path difference caused by the excavation unloading and removal of rock debris by circulating fluid and drilling vibration. In the PS tests, the rock in the vicinity of the borehole undergoes continuous stress adjustments and potential principal stress rotation (Martin 1997; Eberhardt 2001), in contrast to the monotonically increasing stresses in the PD conditions. As a result, additional microcracks are induced in the PS condition due to excavation unloading, which would lead to rock strength degradation (Read et al. 1998; Diederichs et al. 2004; Gu et al. 2023). Moreover, the

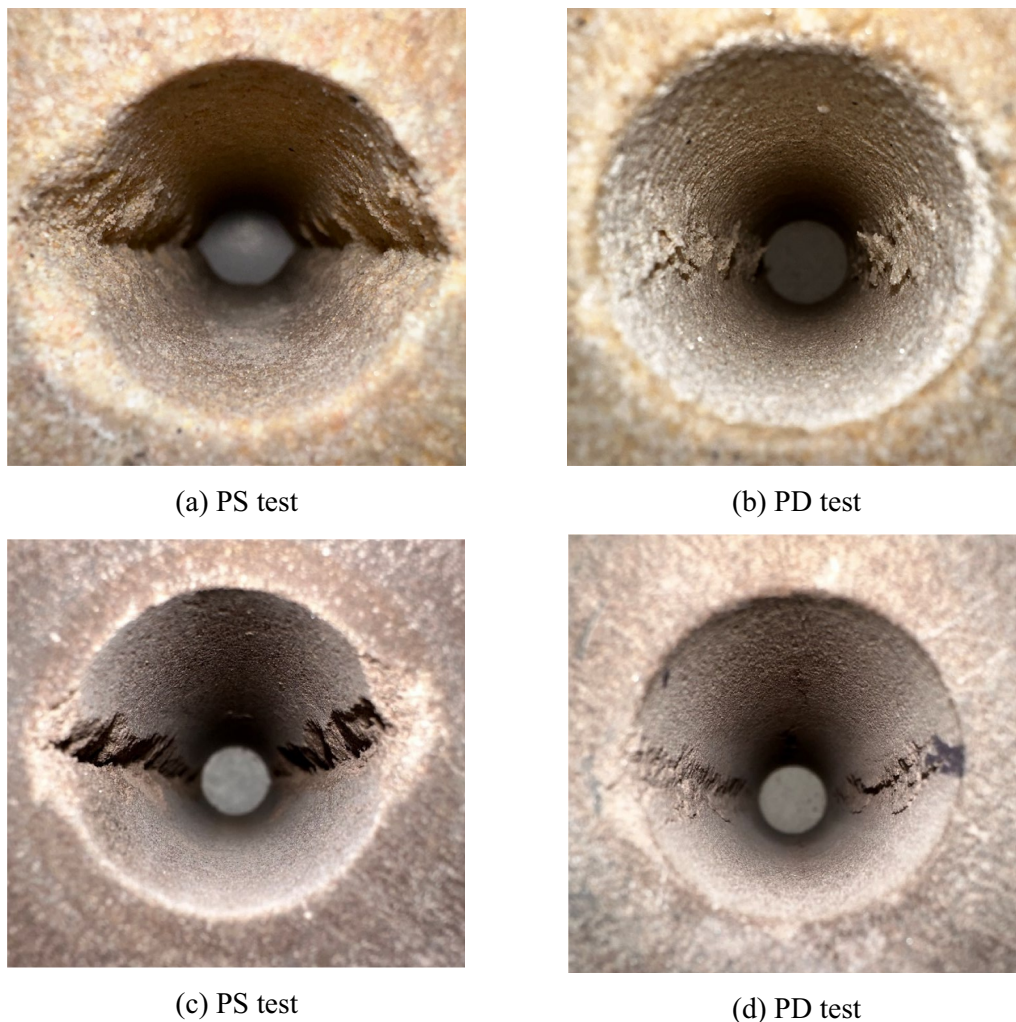


Fig. 7 **a** and **b** borehole breakout images in GSS under $\sigma_H=70$ MPa, $\sigma_h=25$ MPa, $\sigma_v=20$ MPa; **c** and **d** borehole breakout images in YMS under $\sigma_H=90$ MPa, $\sigma_h=15$ MPa, $\sigma_v=10$ MPa

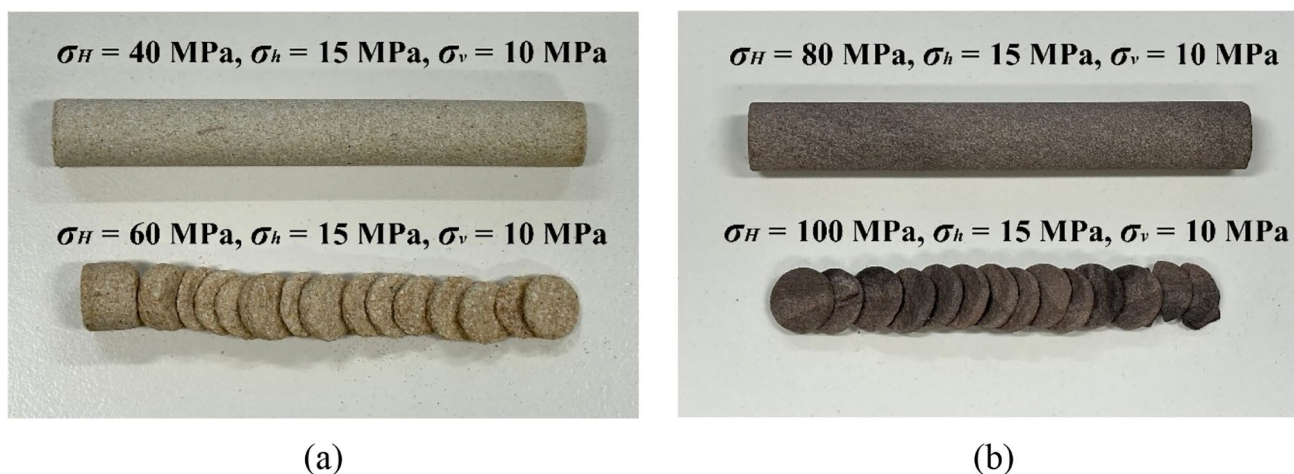


Fig. 8 Core discing observed in a GSS and b YMS PS tests

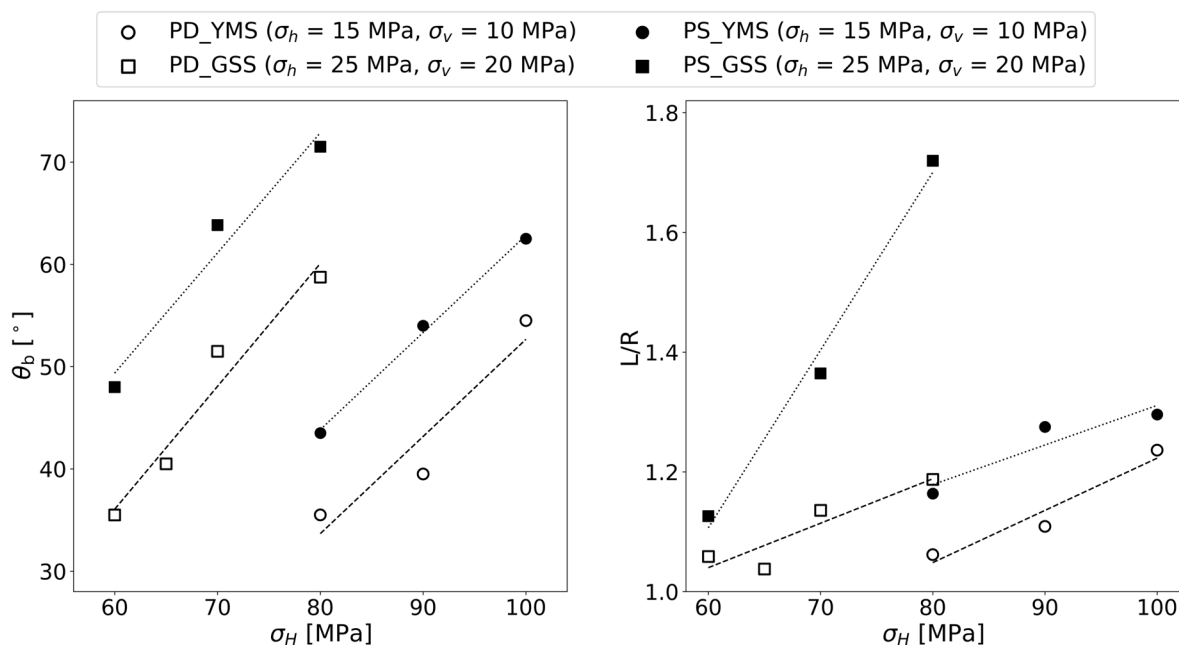


Fig. 9 Comparison of breakout geometries between the PD and PS tests under varying σ_H

rock debris remaining within the failure zones (Figs. 7b, d) could restrain the breakout development under the PD conditions by elevating the minimum stress while reducing the maximum stress acting on the rock surrounding the breakout (Cheatham 1993; Xiang et al. 2023a). In contrast, the cohesionless debris was removed by drilling fluid and vibration in the PS experiments, which facilitates the breakout propagation. Given that the amount of rock debris ejected from the failure area in YMS was generally greater than that in GSS, drilling fluid/vibration would remove less debris in the mudstone. Consequently, the impact of debris removal is more pronounced in GSS than in YMS, as evidenced by

the relatively constant L/R differences in the mudstone as opposed to the increasing L/R differences in the sandstone at high stress (Fig. 9).

The above results suggest that different testing methods could lead to varied stress paths and consequently distinct failure geometries. Compared to the PD experiment, the PS breakout profiles are more consistent with the field observations, and the experimental procedure more closely resembles the in-situ drilling practices. Therefore, the PS method is employed for the following parametric analyses on the correlation between breakout geometries and far-field stresses.

3.2 Impacts of Each Principal Stress on Breakout Geometries

The correlation between σ_H and the extent of breakout and spalling has been well-documented in past studies (Haimson and Lee 2004; Lee 2005; Lee et al. 2016). However, the impacts of σ_h and, particularly, the out-of-plane principal stress (σ_v), were not thoroughly assessed. In this section, the relationships between the breakout geometries and each principal stress were systematically evaluated based on 36 PS test results in GSS and YMS. The tested stress conditions are listed in Table 2. Given the Australian stress regime (Hillis et al. 1999; Heidbach et al. 2018), most tests were carried out under a reverse faulting regime ($\sigma_H > \sigma_h > \sigma_v$) with a few tests in a strike-slip faulting stress regime ($\sigma_H > \sigma_v > \sigma_h$). The stress conditions were selected so that the impact of each principal stress could be assessed individually by varying one principal stress at least three times while keeping the other two stresses constant. The borehole radius and drilling-related variables remained consistent for all tests.

Figure 10 exhibits the extracted breakout geometric parameters for all the stress conditions listed in Table 2. The correlation between each principal stress and breakout geometries is characterised by seven sets of data (six sets in GSS and one set in YMS). In general, all three principal stresses have various degrees of impact on the extent of the breakout in both rock types. σ_H exhibits strong positive correlations with both θ_b and L/R , and the correlations closely approximate linear relationships. The growth rate of L/R tends to increase with the confining stresses. Furthermore, the slopes of YMS for both geometries are smaller compared to those in GSS under the same confinement ($\sigma_h = 15$ MPa, $\sigma_v = 10$ MPa). On the other hand, increases in either σ_h or σ_v restrained the breakout extent in both rock types (Figs. 10b, c), meaning both the in-plane minimum principal stress and out-of-plane stress could affect the borehole failure and spalling.

Among the three principal stresses, σ_H has the most predominant effect on the extent of the breakout. In GSS, variations of 10 MPa in σ_H would lead to average changes of 9° – 15° and 0.16–0.24 in θ_b and L/R , respectively. Whereas the values are slightly smaller in YMS, ranging from 8.5° to 10.5° in θ_b and 0.02 to 0.1 in L/R . The magnitudes of the effects of σ_h and σ_v are very similar, both of which are less significant than that of σ_H . 10 MPa changes in either σ_h or σ_v would result in average variations of 1.5° to 6° and 0.06 to 0.09 in θ_b and L/R in GSS, respectively. For YMS, the corresponding values are 2° to 9.5° for θ_b and 0.004–0.06 for L/R . It is important to note that the elevated σ_v could promote breakout and spalling development, which will be discussed in Sect. 4.2. However, due to the relatively small magnitudes of σ_v compared to σ_H , as constrained by the loading capacity

Table 2 Applied far-field stress magnitudes in the PS borehole breakout experiments

	σ_H (MPa)	σ_h (MPa)	σ_v (MPa)
GSS	40	15	10
	50	15	10
	50	15	15
	50	20	15
	50	27	15
	50	15	20
	55	25	20
	60	15	10
	60	15	20
	60	15	30
	60	25	10
	60	25	20
	60	25	30
	60	35	20
	60	35	30
	70	15	20
	70	25	20
	70	35	20
	70	25	10
	70	25	30
	70	35	30
	70	35	35
	70	15	30
	80	15	20
	80	25	20
80	35	20	
80	25	30	
80	25	36	
80	35	30	
YMS	80	15	10
	90	15	10
	90	15	20
	90	15	30
	90	25	20
	90	35	20
	100	15	10

of the testing system, this effect was not observed in the experiments.

4 Discussion

4.1 Correlation Between θ_b and L/R

Based on the results from Sect. 3.2, both breakout geometries exhibit similar trends with stress variations, and the correlations are mostly linear. As mentioned in Sect. 1, it

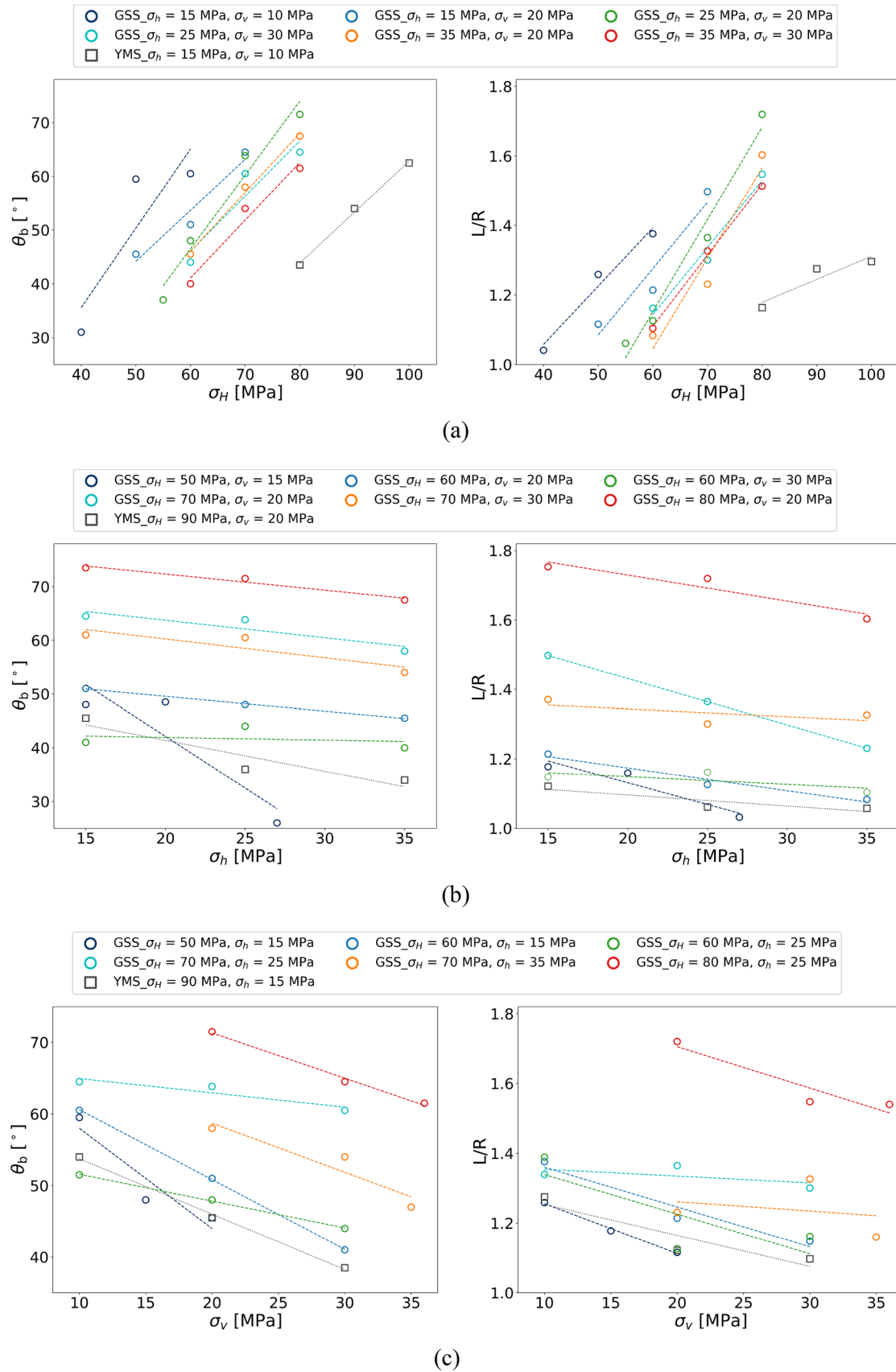


Fig. 10 Variation of breakout geometries as a function of **a** σ_H , **b** σ_h , and **c** σ_v

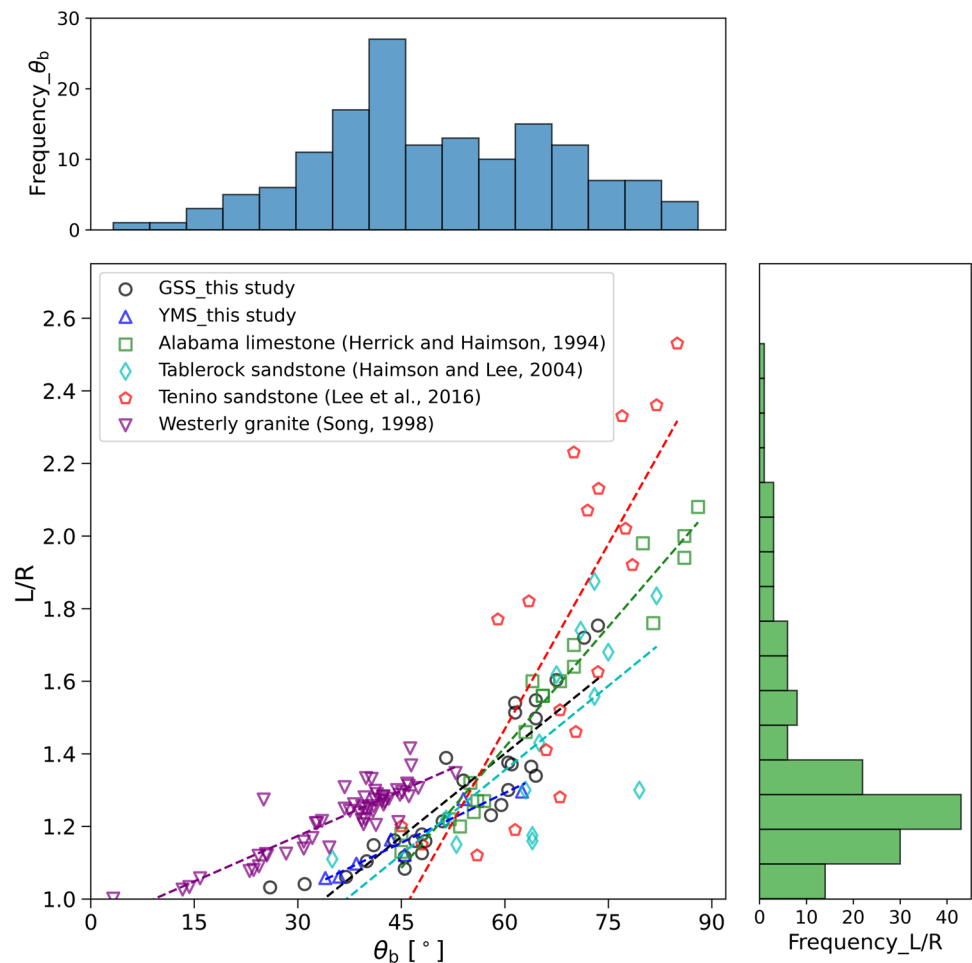
has been suggested by previous studies that there could be a unique relation between θ_b and L/R , which is insensitive to the applied stress magnitudes. If such an exclusive relationship exists, only one principal stress component could be theoretically estimated from breakout geometries. This section evaluates the correlation between θ_b and L/R based on the experimental results from Sect. 3.2 and four additional PS datasets (109 data) collected from the literature on Alabama limestone (Herrick and Haimson 1994), Tablerock sandstone (Haimson and Lee 2004), Tenino sandstone (Lee et al. 2016), and Westerly granite (Song 1998). Note that five data in Tablerock sandstone were excluded from the analysis as their θ_b values exceed 90° .

Figure 11 illustrates the relationship between θ_b and L/R and their distributions across the six datasets. In general, a positive correlation can be found between θ_b and L/R , which breakout and spalling tend to widen and deepen simultaneously. Within each dataset, the correlation could be reasonably approximated through a linear fitting. However, as depicted in the figure, the frequency distribution patterns for the two geometries exhibited notable differences. The θ_b distribution aligns with a normal distribution pattern, with

the majority of data exceeding 30° and the peak frequency occurring around 40 to 45° . In contrast, the L/R data cluster towards lower values, concentrating mostly between 1.1 to 1.4 . The data distribution follows closely to a positive skew pattern. Moreover, the data in different datasets are spread out, and the relationships between θ_b and L/R vary depending on the rock properties and stress magnitudes. A universal linear correlation, similar to those obtained from single rock types, could not be established across all datasets. Even within each subset, a single value of one geometry could correspond to multiple values of the other geometry depending on the applied stresses. For instance, in GSS, experiments with $\sigma_H=70$ MPa, $\sigma_h=25$ MPa, $\sigma_v=10$ MPa and $\sigma_H=80$ MPa, $\sigma_h=25$ MPa, $\sigma_v=30$ MPa both yielded θ_b values of 64.5° , whereas L/R differed at 1.34 and 1.55 , respectively. Similarly, in Tablerock sandstone, L/R for experiments under $\sigma_H=60$ MPa, $\sigma_h=20$ MPa, $\sigma_v=40$ MPa and $\sigma_H=65$ MPa, $\sigma_h=30$ MPa, $\sigma_v=40$ MPa was consistent at 1.3 , whereas θ_b was 63° and 79.5° , respectively.

This could be attributed to the differences in the formation mechanisms for θ_b and L/R , as discussed in Xiang et al. (2023b). The width of the breakout forms in the initial stage

Fig. 11 Correlations and frequency distributions of θ_b and L/R across six datasets



of the breakout development, primarily driven by the extensile failure mechanism (Bažant et al. 1993; Haimson 2007; Xiang et al. 2023c), and its value remains relatively constant in subsequent breakout propagation (Zoback et al. 1985; Zheng et al. 1989; Duan and Kwok 2016). The formation and stabilisation mechanism can be adequately simplified based on the elastic theory. On the other hand, the failure depth development is a progressive progress (Haimson 2007; Liu et al. 2017; Xiang et al. 2023a). Its evolution is more complicated involving plastic damage and rock residual properties (Cheatham 1993; Perras and Diederichs 2016; Xiang et al. 2023b). The same stabilisation mechanism that applies θ_b could not effectively be extended to L/R . Consequently, the two geometries could have varied sensitivities to the applied stresses.

The above analysis indicates that although both breakout parameters show similar correlations with the stress magnitudes, these correlations vary across rock types and applied stresses. Consequently, the argument that a unique relationship exists between θ_b and L/R may not be valid. For geotechnical analysis involving borehole breakout and spalling, it is recommended to utilise both geometrical parameters, as they can be readily obtained through borehole loggings or site surveys. Additionally, in terms of in-situ stress estimation, it should be viable to derive two principal stress components when both θ_b and L/R are employed.

4.2 Correlation Between Far-Field Stresses and Breakout Dimensions

Understanding the correlation between the in-situ stresses and the extent of borehole breakout and spalling is critical in various engineering applications. The σ_1 magnitude and its ratio to rock strength have been widely applied for the

evaluation and prediction of the spalling and strain bursting phenomenon (Barton et al. 1974; Zhou et al. 2018; He et al. 2023; Gong et al. 2023). Furthermore, the depth of spalling was found to be closely related to the maximum tangential stress (σ_{max}) around the excavation (Martin et al. 1999). A simple empirical relation (Eq. (1)) was proposed to estimate the spalling depth based on the ratio of σ_{max} to the rock critical/spalling strength (σ_c), which has been broadly adopted in excavation stability assessment and support design (Martin et al. 1999; Martin and Christiansson 2009). However, while these criteria can reasonably approximate the potential and extent of breakout and spalling, they only consider the in-plane stress components. Whereas the failure around openings is affected by all three principal stresses based on the analysis in Sect. 3.2. Take the experimental results in GSS for example, relatively good correlations can be observed between σ_{max} and the breakout geometries (Fig. 12). Nonetheless, multiple breakout values could be associated with the same σ_{max} (e.g., 135 MPa). Therefore, the out-of-plane stress should be considered for better characterising the breakout and spalling.

$$L/R = 0.5 \frac{\sigma_{max}}{\sigma_c} + 0.48 \pm 0.1 \quad (1)$$

where $\sigma_{max} = 3 \times \sigma_H - \sigma_h$.

At the direction of σ_h , the stress state in the vicinity of the borehole is close to the biaxial loading states with $\sigma_1 \approx \sigma_{max}$, $\sigma_2 =$ out-of-plane stress (σ_v), $\sigma_3 \approx 0$. Extensive polyaxial experiments have revealed that σ_2 has considerable impacts on rock strength (Mogi 1967; Haimson and Chang 2000; Colmenares and Zoback 2002). At relatively low σ_2 , the cracks could propagate along the $\sigma_1 - \sigma_2 / \sigma_3$

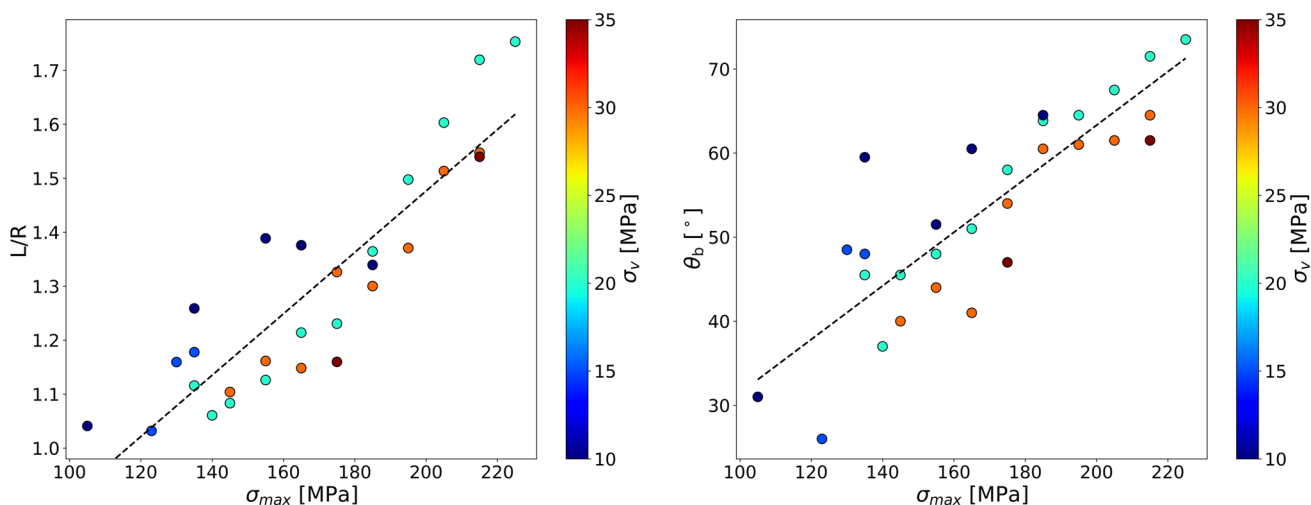


Fig. 12 Correlations between σ_{max} and the breakout geometries in GSS

planes due to high differential stresses in these planes. Increasing σ_2 could constrain the crack propagation and coalescence in the σ_1 - σ_3 direction, leading to an increase in σ_c and decreases in breakout geometries. However, as σ_2 continues increasing, the elevated differential stress along the σ_2 - σ_3 plane would increase the extensile strain towards the open face, promoting tensile cracks development in the σ_1 - σ_2 plane. Consequently, the strengthening effect of σ_2 on σ_c is replaced by a weakening effect under relatively high σ_2 . Furthermore, the breakout and spalling formation process has been well recognised to be closely related to the rock crack initiation (σ_{ci}) and crack damage (σ_{cd}) stresses (Martin et al. 1994; Diederichs 2007; Mahmoud 2023), both of which also exhibit increasing and then decreasing correlations with σ_2 (Kong et al. 2018). Therefore, to incorporate the impact of σ_2 , the following quadratic polynomial (Eq. (2)) is adopted to empirically correlate the stresses with the failure geometries, as suggested by Su et al. (2023), which is then compared to the correlations based solely on σ_{max} (Eq. (3))

$$\text{Breakout geometries} = A(\sigma_{max}) + B(\sigma_v)^2 + C(\sigma_v) + D \quad (2)$$

$$\text{Breakout geometries} = A'(\sigma_{max}) + B' \quad (3)$$

where A, B, C, D, A' and B' are the fitting parameters.

The experimental results in GSS are used as examples and analysed in detail. The fitted equations for the breakout geometries based on Eq. (2) and their comparisons with those based on Eq. (3) are presented in Fig. 13. Note that the θ_b correlation may yield a small θ_b value even under relatively low stresses when the breakout is not initiated, in contrast to the L/R correlation, where a value ≤ 1 indicates that the failure is not initiated. This is attributed to the data characteristics, wherein L/R starts from 1 while θ_b begins from 0° with most values exceeding 30° (Fig. 11). As a result, the correlation for θ_b cannot be applied to assess breakout initiation and should be employed only when the estimated $L/R > 1$. In general, the empirical models incorporated σ_v better represent breakout and spalling dimensions under various stress conditions. The coefficients of determination (R^2) for L/R and θ_b are improved from 0.79 and 0.72 to 0.89 and 0.85, respectively. The root mean squared errors ($RMSE$) for the two geometries also exhibit improvement, decreasing from 0.092 and 6.17 to 0.066 and 4.55, respectively. Furthermore, the issue of multiple breakout values corresponding to the same σ_{max} (Fig. 12) is effectively addressed by Eq. (2). Note that the strength-weakening effect of high σ_2 was not distinctly observed for the dataset, which is attributed to the applied σ_v being relatively small as the applied stresses in most experiments were under the reverse faulting regime (Table 2).

The fitting performance for the remaining datasets utilised in Sect. 4.1 is summarised in Table 3. Empirical correlations based on σ_{max} can yield satisfactory results in various rock types, except for YMS and Westerly granite. Nonetheless, consistent improvement can be observed across all datasets through Eq. (2). This indicates that although the failure around the borehole is dominant by σ_{max} , incorporating the out-of-plane stress provides a more accurate representation of the failure characteristics.

To further generalise the correlations, the stress values in Eq. (3) are normalised by σ_c . Since all the data analysed in this study are obtained from laboratory experiments on 22 mm boreholes, the following empirical equation from Lin et al. (2021) is applied to calculate the borehole wall strength (BWS), which is then used as σ_c .

$$BWS = (0.0005R^2 - 0.0638R + 2.7885)UCS \quad (4)$$

The generalised empirical correlations for L/R and θ_b , based on Eqs. (2) and (3) are given in Eqs. (5), (6), (7), (8) respectively. Notably, Eq. (5) closely resembles the empirical correlation derived from in-situ spalling data (Eq. (1)). Similar to the θ_b correlation shown in Fig. 13, Eqs. (6) and (8) should be used only when the estimated L/R is greater than 1. As indicated in Fig. 14, the abovementioned strengthening and weakening effects of σ_2 (σ_v) are observed in both geometries, meaning the empirical correlations based solely on σ_{max} may either underestimate or overestimate the failure extent depending on the σ_2 magnitudes. In comparison to Eqs. (5), (6), (7), (8) better correlate the far-field stresses and breakout dimensions, with R^2 values improved from 0.47 to 0.62 and 0.59 to 0.68, respectively. Furthermore, the weights of σ_{max} and σ_v in Eq. (7) differ compared to those of Eq. (8) which further indicates that the θ_b and L/R have varied correlations with the stress magnitudes.

$$L/R = 0.4301 \frac{\sigma_{max}}{\sigma_c} + 0.6267 \quad (5)$$

$$\theta_b = 27.24 \frac{\sigma_{max}}{\sigma_c} + 4.16(\text{if } L/R > 1) \quad (6)$$

$$L/R = 0.3977 \frac{\sigma_{max}}{\sigma_c} + 2.9286 \left(\frac{\sigma_v}{\sigma_c} \right)^2 - 1.5259 \frac{\sigma_v}{\sigma_c} + 0.809 \quad (7)$$

$$\theta_b = 22.21 \frac{\sigma_{max}}{\sigma_c} + 72.35 \left(\frac{\sigma_v}{\sigma_c} \right)^2 - 16.66 \frac{\sigma_v}{\sigma_c} + 10.36(\text{if } L/R > 1) \quad (8)$$

However, it is important to note that the data points in Fig. 14 are relatively scattered, and the fitting results for Eqs. (7) and (8) are generally not as satisfactory as those

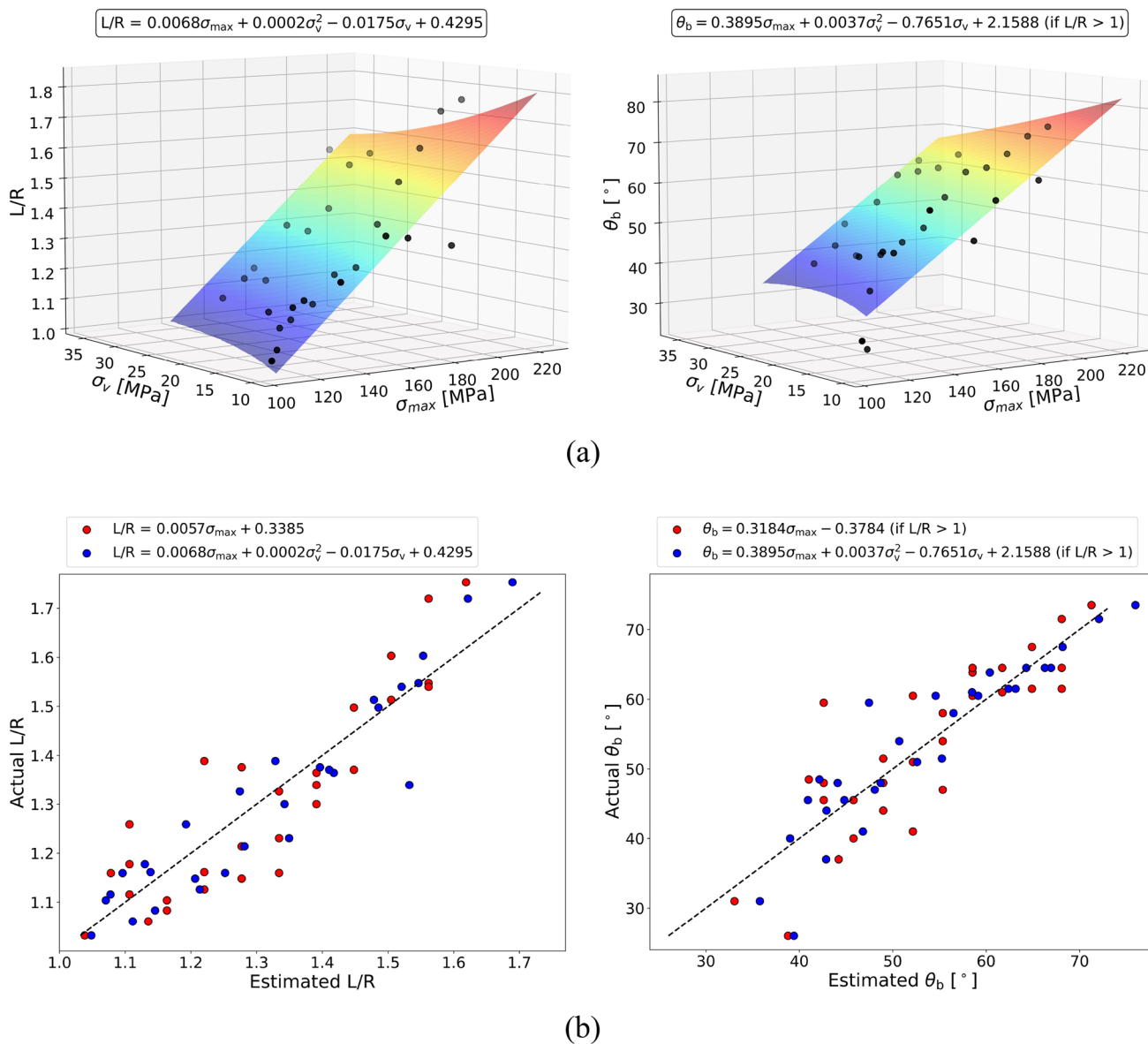


Fig. 13 a Empirical correlations based on Eq. (2) in GSS, and b their comparisons against fittings based on Eq. (3)

Table 3 Fitting performance comparisons between the Eq. (3) and Eq. (2)

Dataset	Equation (3)				Equation (2)			
	L/R_{R^2}	L/R_{RMSE}	$\theta_b_{R^2}$	θ_b_{RMSE} (°)	L/R_{R^2}	L/R_{RMSE}	$\theta_b_{R^2}$	θ_b_{RMSE} (°)
GSS	0.79	0.092	0.72	6.17	0.89	0.066	0.85	4.55
YMS	0.37	0.072	0.56	6.33	0.96	0.017	0.97	1.77
Alabama limestone (Herrick and Haimson 1994)	0.79	0.136	0.78	6.15	0.93	0.080	0.91	3.83
Tablerock sandstone (Haimson and Lee 2004)	0.87	0.096	0.76	5.84	0.88	0.092	0.79	5.49
Tenino sandstone (Lee et al. 2016)	0.73	0.232	0.71	5.66	0.76	0.218	0.91	3.16
Westerly granite (Song 1998)	0.56	0.06	0.39	7.66	0.63	0.055	0.47	7.09

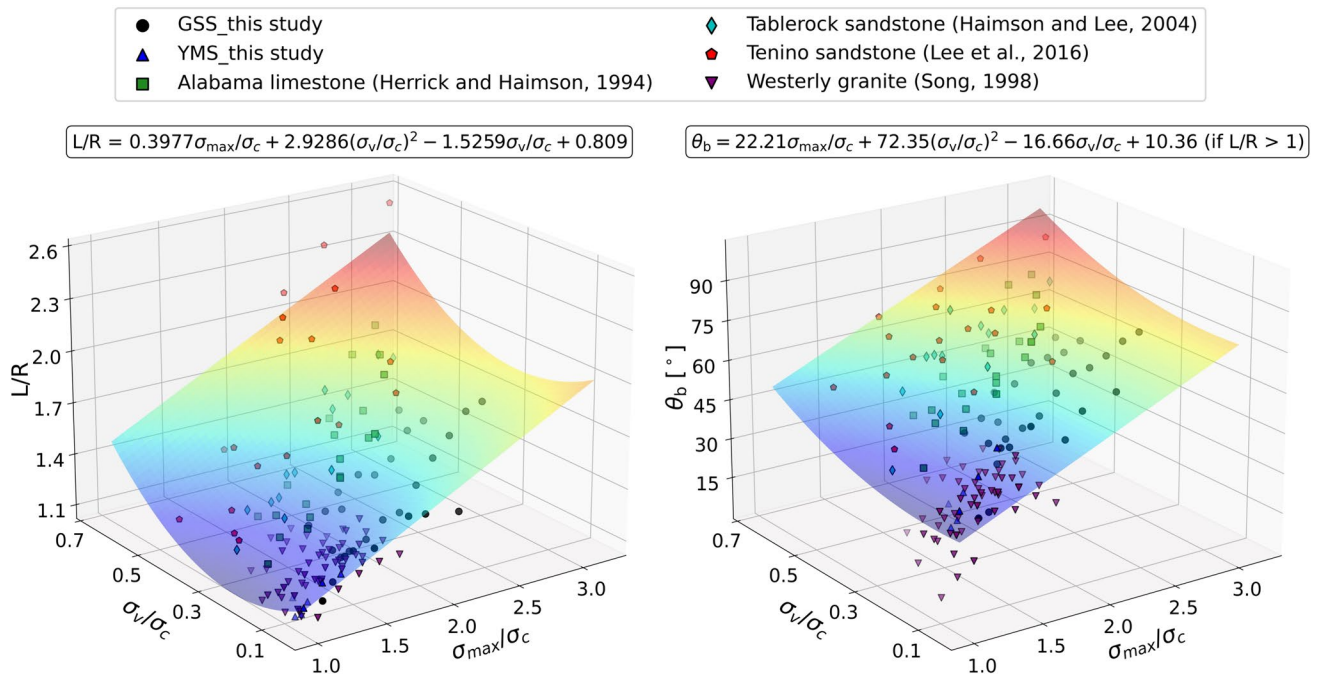


Fig. 14 Breakout geometries as functions of σ_{max}/σ_c and σ_v/σ_c

for individual rock types (Table 3). This suggests that there could be additional material properties apart from rock strength contributing to the breakout and spalling phenomena. Moreover, the impacts of excavation unloading and removal of rock debris on the breakout formation could vary across different rock types as demonstrated in Sect. 3.1. Further investigations are still required to enhance the generalisation of the empirical correlations and their practical applicability.

5 Conclusions

In this study, the borehole breakout and spalling phenomena in two rock types were investigated through true-triaxial experiments. The tests were carried out based on two methodologies (PD and PS) on cubic rock specimens (120 mm \times 120 mm \times 120 mm) with $\Phi 22$ mm boreholes. The main conclusions of this study are summarised below.

1. Borehole recordings revealed that the breakout formation characteristics are different between GSS and YMS. The breakout in the former primarily occurred as the buckling deformation with protruding rock debris, while the failure of the latter is more intense involving ejections of rock grains and slabs. Compared with the PD experiments, PS experiments consistently yielded wider and deeper breakouts, indicating that the effects of exca-

vation-unloading and removal of rock debris are evident in both rock types.

2. The impact of each principal stress on the failure dimensions was assessed based on 36 PS experiments. The results indicate that the extent of borehole breakout is affected by all three principal stresses, among which σ_H has the most prominent influence on the failure geometries. In comparison, the impacts of σ_h and σ_v are less significant. Nonetheless, both of them could still result in considerable changes in failure dimensions, and thus, it is important to consider all three principal stresses in characterising the breakout and spalling.

3. The correlations between θ_b and L/R and whether there exists a unique correlation between the two breakout geometries were investigated through six PS datasets from this study and the literature. While both geometries tend to increase/decrease simultaneously, their formation mechanisms fundamentally differ. A universal linear correlation, similar to those derived from individual rock types, could not be established across various rock types, and their data distributions exhibit notably varied patterns. Moreover, a single value of one geometry could be associated with several values of the other geometry in the same rock type under varied applied stresses. Therefore, the correlation between θ_b and L/R does not appear to be unique, making it feasible to derive two principal stress components from the breakout geometries.

4. Given the impacts of the out-of-plane stress on breakout and spalling, σ_v was incorporated into empirical cor-

relations with σ_{max} in the forms of quadratic polynomials to characterise breakout dimensions. Compared to those based solely on σ_{max} , the proposed correlations could more accurately evaluate both θ_b and L/R under various stress conditions across all datasets, which would be beneficial for the stability analysis of underground excavations (e.g., tunnel, borehole, and nuclear waste repository).

Acknowledgements The work reported here is funded by the Australian Coal Industry's Research Program (ACARP), Grant no. C26063. The authors would also like to acknowledge the technical support in laboratory tests from Kanchana Gamage and Mark Whelan at UNSW.

Funding Open Access funding enabled and organized by CAUL and its Member Institutions. Open Access funding enabled and organized by CAUL and its Member Institutions. Australian Coal Industry's Research Program (ACARP), Grant no. C26063, Jounq Oh.

Data availability Upon request, data would be available.

Declarations

Conflict of interest The authors declare that they have no known competing financial interests or personal relationships that could have appeared to influence the work reported in this paper.

Open Access This article is licensed under a Creative Commons Attribution 4.0 International License, which permits use, sharing, adaptation, distribution and reproduction in any medium or format, as long as you give appropriate credit to the original author(s) and the source, provide a link to the Creative Commons licence, and indicate if changes were made. The images or other third party material in this article are included in the article's Creative Commons licence, unless indicated otherwise in a credit line to the material. If material is not included in the article's Creative Commons licence and your intended use is not permitted by statutory regulation or exceeds the permitted use, you will need to obtain permission directly from the copyright holder. To view a copy of this licence, visit <http://creativecommons.org/licenses/by/4.0/>.

References

- Andersson JC, Martin CD (2009) The Äspö pillar stability experiment: part i—experiment design. *Int J Rock Mech Min Sci* 46:865–878
- Andersson JC, Martin CD, Stille H (2009) The äspö pillar stability experiment: part ii—rock mass response to coupled excavation-induced and thermal-induced stresses. *Int J Rock Mech Min Sci* 46:879–895
- Barton N, Lien R, Lunde J (1974) Engineering classification of rock masses for the design of tunnel support. *Rock Mech* 6:189–236
- Barton CA, Zoback MD, Burns KL (1988) In-situ stress orientation and magnitude at the fenton geothermal site, New Mexico, determined from wellbore breakouts. *Geophys Res Lett* 15:467–470
- Bažant ZP, Lin F, Lippmann H (1993) Fracture energy release and size effect in borehole breakout. *Int J Numer Anal Methods Geomech* 17:1–14
- Bieniawski ZT, Bernede MJ (1979) Suggested methods for determining the uniaxial compressive strength and deformability of rock materials: part 1. Suggested method for determining deformability of rock materials in uniaxial compression. *Int J Rock Mech Min Sci Geomech Abstr* 16:138–140
- Bieniawski ZT, Hawkes I (1978) Suggested methods for determining tensile strength of rock materials. *Int J Rock Mech Min Sci Geomech Abstr* 15:99–103
- Borm G, Engeser B, Hoffers B et al (1997) Borehole instabilities in the KTB main borehole. *J Geophys Res Solid Earth* 102:18507–18517
- Cheatham JB (1993) A new hypothesis to explain stability of borehole breakouts. *Int J Rock Mech Min Sci Geomech Abstr* 30:1095–1101
- Cheon D-S, Jeon S, Park C et al (2011) Characterization of brittle failure using physical model experiments under polyaxial stress conditions. *Int J Rock Mech Min Sci* 48:152–160
- Colmenares LB, Zoback MD (2002) A statistical evaluation of intact rock failure criteria constrained by polyaxial test data for five different rocks. *Int J Rock Mech Min Sci* 39:695–729
- Cox JW (1972) The high-resolution dipmeter reveals dip-related borehole and formation characteristics. In: SPWLA 11th Annual Logging Symposium. Society of Petrophysicists and Well-Log Analysts
- Diederichs MS (2007) The 2003 Canadian geotechnical colloquium: mechanistic interpretation and practical application of damage and spalling prediction criteria for deep tunnelling. *Can Geotech J* 44:1082–1116
- Diederichs MS, Kaiser PK, Eberhardt E (2004) Damage initiation and propagation in hard rock during tunnelling and the influence of near-face stress rotation. *Int J Rock Mech Min Sci* 41:785–812
- Duan K, Kwok C (2016) Evolution of stress-induced borehole breakout in inherently anisotropic rock: insights from discrete element modeling. *J Geophys Res Solid Earth* 121:2361–2381
- Eberhardt E (2001) Numerical modelling of three-dimension stress rotation ahead of an advancing tunnel face. *Int J Rock Mech Min Sci* 38:499–518
- Emmermann R, Lauterjung J (1997) The German continental deep drilling program ktb: overview and major results. *J Geophys Res Solid Earth* 102:18179–18201
- Feng X-T, Xu H, Qiu S-L et al (2018) In Situ Observation of rock spalling in the deep tunnels of the china jinping underground laboratory (2400 m depth). *Rock Mech Rock Eng* 51:1193–1213
- Feng X-T, Haimson B, Li X et al (2019) ISRM Suggested method: determining deformation and failure characteristics of rocks subjected to true triaxial compression. *Rock Mech Rock Eng* 52:2011–2020
- Franklin JA (1979) Suggested methods for determining water content, porosity, density, absorption and related properties and swelling and slake-durability index properties. *Int J Rock Mech Min Sci Geomech Abstr* 16:141–156
- Gong F, Dai J, Xu L (2023) A strength-stress coupling criterion for rockburst: inspirations from 1114 rockburst cases in 197 underground rock projects. *Tunn Undergr Space Technol* 142:105396
- Gough D, Bell J (1981) Stress orientations from oil-well fractures in Alberta and Texas. *Can J Earth Sci* 18:638–645
- Gu L, Feng X-T, Kong R et al (2023) Excavation stress path induced fracturing mechanism of hard rock in deep tunnel. *Rock Mech Rock Eng* 56:1779–1806
- Haimson B (2007) Micromechanisms of borehole instability leading to breakouts in rocks. *Int J Rock Mech Min Sci* 44:157–173
- Haimson B, Chang C (2000) A new true triaxial cell for testing mechanical properties of rock, and its use to determine rock strength and deformability of Westerly granite. *Int J Rock Mech Min Sci* 37:285–296
- Haimson B, Lee H (2004) Borehole breakouts and compaction bands in two high-porosity sandstones. *Int J Rock Mech Min Sci* 41:287–301

- Haimson B, Lee M, Herrick C (1991) Recent advances In: in-situ stress measurements by hydraulic fracturing and borehole breakouts. Paper presented at the 7th ISRM Congress, Aachen, Germany
- Han H, van der Baan M (2024) Constraint strategies for estimating in-situ stress from borehole measurements. *Geomech Energy Environ* 37:100518
- He M, Cheng T, Qiao Y, Li H (2023) A review of rockburst: experiments, theories, and simulations. *J Rock Mech Geotech Eng* 15:1312–1353
- Heidbach O, Rajabi M, Cui X et al (2018) The world stress map database release 2016: crustal stress pattern across scales. *Tectonophysics* 744:484–498
- Herrick CG, Haimson BC (1994) Modeling of episodic failure leading to borehole breakouts in Alabama limestone. Presented at the 1st North American Rock Mechanics Symposium, Austin, Texas
- Hillis RR, Enever JR, Reynolds SD (1999) In situ stress field of eastern Australia. *Aust J Earth Sci* 46:813–825
- Hoek E, Martin C (2014) Fracture initiation and propagation in intact rock—a review. *J Rock Mech Geotech Eng* 6:287–300
- Hu X, Su G, Chen G et al (2019) Experiment on rockburst process of borehole and its acoustic emission characteristics. *Rock Mech Rock Eng* 52:783–802
- Kong R, Feng X-T, Zhang X, Yang C (2018) Study on crack initiation and damage stress in sandstone under true triaxial compression. *Int J Rock Mech Min Sci* 106:117–123
- Lee H (2005) Borehole breakouts in arkosic sandstones and quartz-rich sandstones. The University of Wisconsin, Madison
- Lee M, Haimson B (1993) Laboratory study of borehole breakouts in Lac du Bonnet granite: a case of extensile failure mechanism. *Int J Rock Mech Min Sci Geomech Abstr* 30:1039–1045
- Lee H, Moon T, Haimson BC (2016) Borehole breakouts induced in arkosic sandstones and a discrete element analysis. *Rock Mech Rock Eng* 49:1369–1388
- Lin H, Singh S, Oh J et al (2020) A combined approach for estimating horizontal principal stress magnitudes from borehole breakout data via artificial neural network and rock failure criterion. *Int J Rock Mech Min Sci* 136:104539
- Lin H, Oh J, Canbulat I et al (2021) Experimental study on borehole size effect and prediction of breakout initiation stress. *Int J Rock Mech Min Sci* 142:104762
- Ling K, Wang Y, Liu D et al (2023) Experimental study on rockburst and spalling failure in circular openings for deep underground engineering. *Rock Mech Rock Eng* 56:2607–2631
- Liu G, Feng X-T, Jiang Q et al (2017) In situ observation of spalling process of intact rock mass at large cavern excavation. *Eng Geol* 226:52–69
- Mahmoud M (2023) Physical modelling of spalling failure in underground structures. The University of Queensland, St Lucia QLD
- Martin CD (1997) Seventeenth canadian geotechnical colloquium: the effect of cohesion loss and stress path on brittle rock strength. *Can Geotech J* 34:698–725
- Martin CD, Christiansson R (2009) Estimating the potential for spalling around a deep nuclear waste repository in crystalline rock. *Int J Rock Mech Min Sci* 46:219–228
- Martin CD, Martino JB, Dzik EJ (1994) Comparison of borehole breakouts from laboratory and field tests. Proceedings Eurock'94 SPE/ISRM rock mechanics in petroleum engineering conference. A A Balkema, Delft, Rotterdam, pp 183–190
- Martin CD, Read RS, Martino JB (1997) Observations of brittle failure around a circular test tunnel. *Int J Rock Mech Min Sci* 34:1065–1073
- Martin CD, Kaiser PK, McCreath DR (1999) Hoek-Brown parameters for predicting the depth of brittle failure around tunnels. *Can Geotech J* 36:136–151
- Martin CD, Christiansson R, Soederhaell J (2001) Rock stability considerations for siting and constructing a KBS-3 repository. University of Alberta, SKB TR-01-38, Sweden
- Mogi K (1967) Effect of the intermediate principal stress on rock failure. *J Geophys Res* 72:5117–5131
- Perras MA, Diederichs MS (2016) Predicting excavation damage zone depths in brittle rocks. *J Rock Mech Geotech Eng* 8:60–74
- Read R (2004) 20 years of excavation response studies at AECL's underground research laboratory. *Int J Rock Mech Min Sci* 41:1251–1275
- Read R, Chandler N, Dzik E (1998) In situ strength criteria for tunnel design in highly-stressed rock masses. *Int J Rock Mech Min Sci* 35:261–278
- Sahara DP, Schoenball M, Gerolymatou E, Kohl T (2017) Analysis of borehole breakout development using continuum damage mechanics. *Int J Rock Mech Min Sci* 97:134–143
- Si X, Li X, Gong F et al (2022) Experimental investigation of failure process and characteristics in circular tunnels under different stress states and internal unloading conditions. *Int J Rock Mech Min Sci* 154:105116
- Song I (1998) Borehole breakouts and core dishing in Westerly granite: mechanisms of formation and relationship to in situ stress. The University of Wisconsin, Madison
- Song I, Chang C (2018) Stochastic optimization of in situ horizontal stress magnitudes using probabilistic model of rock failure at wellbore breakout margin. *Rock Mech Rock Eng* 51:2761–2776
- Stephansson O, Zang A (2012) ISRM suggested methods for rock stress estimation—part 5: establishing a model for the in situ stress at a given site. *Rock Mech Rock Eng* 45:955–969
- Su G, Chen Y, Jiang Q et al (2023) Spalling failure of deep hard rock caverns. *J Rock Mech Geotech Eng* 15:2083–2104
- Tingay M, Reinecker J, Müller B (2008) Borehole breakout and drilling-induced fracture analysis from image logs. World Stress Map Project 1:8
- Xiang Z, Moon T, Oh J et al (2023a) Numerical investigation of borehole breakout and rock spalling based on strain energy criteria. *Int J Rock Mech Min Sci* 171:105587
- Xiang Z, Moon T, Si G et al (2023b) Numerical analysis of v-shaped borehole breakout using three-dimensional discrete-element method. *Rock Mech Rock Eng* 56:3197–3214
- Xiang Z, Moon T, Oh J et al (2023c) Analytical investigations of in situ stress inversion from borehole breakout geometries. *J Rock Mech Geotech Eng*. <https://doi.org/10.1016/j.jrmge.2023.08.018>
- Xiang Z, Si G, Oh J, et al (2023d) Experimental investigation of borehole breakout formation in Gosford sandstone. *Int J Rock Mech Min Sci* (Under review)
- You M (2009) True-triaxial strength criteria for rock. *Int J Rock Mech Min Sci* 46:115–127
- Zheng Z, Kemeny J, Cook NG (1989) Analysis of borehole breakouts. *J Geophys Res Solid Earth* 94:7171–7182
- Zhou J, Li X, Mitri HS (2018) Evaluation method of rockburst: state-of-the-art literature review. *Tunn Undergr Space Technol* 81:632–659
- Zoback MD, Moos D, Mastin L, Anderson RN (1985) Well bore breakouts and in situ stress. *J Geophys Res Solid Earth* 90:5523–5530
- Zoback M, Barton C, Brudy M et al (2003) Determination of stress orientation and magnitude in deep wells. *Int J Rock Mech Min Sci* 40:1049–1076

Publisher's Note Springer Nature remains neutral with regard to jurisdictional claims in published maps and institutional affiliations.